EXPERIMENTAL STUDY ON THE ROLE OF FOOTING EMBEDMENT ON TUNNEL-FOUNDATION INTERACTION

Jingmin Xu[1], Andrea Franza[2], Alec M. Marshall[3], and Nunzio Losacco[4]

[1]Assistant Professor, School of Transportation, Southeast Univ., Nanjing, China; formerly, Dept. of Civil Engineering, Univ. of Nottingham, Nottingham, UK. Email: jingmin_xu@seu.edu.cn

[2]Research Fellow, Dept. of Civil and Architectural Engineering, Aarhus Univ., Aarhus, Denmark.

[3]Associate Professor, Dept. of Civil Engineering, Univ. of Nottingham, Nottingham, UK.

[4]Research Fellow, Dept. of Civil, Env., Land, Building Eng. and Chemistry, Polytechnic Univ. of Bari, Bari, Italy.

ABSTRACT

This technical note investigates the effect of footing embedment depth on tunnel-structure interaction using geotechnical centrifuge testing. A two-story framed building on separate footings, either resting directly on the surface or embedded in the soil, and subjected to tunneling induced displacements is modeled. Measurements of the displacements of the footings and underlying soil, ground deformations, and structural distortions are presented. Results show that footing embedment increases foundation differential settlements and horizontal displacements, thereby causing a greater level of distortion within the frame. Furthermore, the embedded footings result in a larger magnitude of ground displacements and shear strains of the soil. Finally, modification factors and relative stiffness parameters are presented, indicating a greater effect of the embedment on horizontal deformations than the angular distortion of the bays.

INTRODUCTION

Prediction of tunneling-induced structural distortions and damage is a necessary stage of urban tunneling projects. When considering a building founded on shallow foundations, it is generally assumed that the foundations rest directly on the surface, both in numerical (Goh and Mair, 2014; Fu et al., 2018) and experimental (Ritter, 2017; Xu et al., 2020b) studies. However, in reality, shallow foundations are usually buried at a certain depth. This aspect has been discussed for foundations

that are continuous in the direction transverse to the tunnel by Losacco et al. (2014); Yiu et al. (2017) and Boldini et al. (2018), however there is a lack of information for separate footings, for which embedment is arguably more important because of the potential for significant horizontal foundation displacements.

To evaluate the impact of footing embedment, this technical note presents results from two plane-strain geotechnical centrifuge tests of tunneling in sand beneath a frame founded on separate footings resting either on the ground surface or embedded within the soil. The investigation aims to provide insights into the role of the foundation embedment and provides high-quality experimental data which may serve as benchmark for more exhaustive numerical analyses.

EXPERIMENTAL DETAILS

The two-story aluminium framed building model in Figure 1(a) with separate strip footings was used. All model building components were bolted together, including additional bars at the wall/slab nodes to achieve fixed-fixed connections. As shown in Figure 1(b), the model building has a transverse width B of 460.4 mm, with a length of 258 mm in the longitudinal direction of the tunnel, similar to the strongbox, to achieve plane-strain conditions. Footing transverse width b_{foot} and bay width b_{bay} are, respectively, 12 mm and 38.1 mm. All walls and slabs have a thickness t =3.2 mm. Each story has the same height h_{story} =38.1 mm , thus giving a total building height H of 79.4 mm. The plane-strain tunneling model described in Xu et al. (2020b) was used, with a flexible membrane model tunnel (diameter D_t = 90 mm), a strongbox with a transparent acrylic front wall, and a tunnel volume loss control system. A fine-grained dry silica sand (Leighton Buzzard Fraction E) was used, with minimum and maximum void ratios of 0.65 and 1.01 (Zhao, 2008; Lanzano et al., 2016). A thin layer of sand was glued to the underside and sides of the footings to obtain a rough surface. The GeoPIV digital image analysis technique (White et al., 2003) was used to measure both soil and structure displacements.

Tests were performed on the Nottingham Centre for Geomechanics 4 m diameter geotechnical centrifuge (Ellis et al., 2006). Two tunnel-building interaction tests were carried out using dense sand (I_d =90%, corresponding to a void ratio of 0.974) with the footings either resting on the

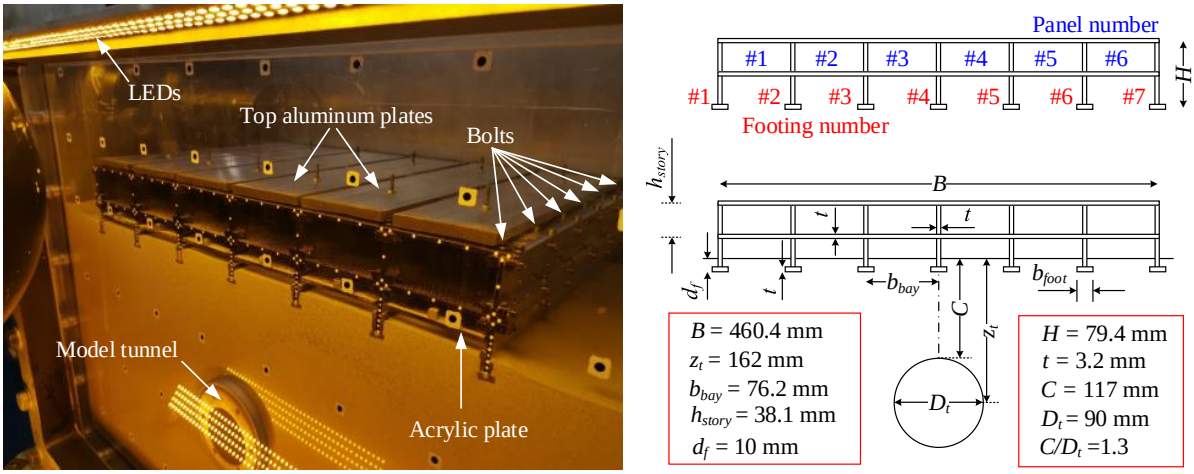

(a) Model setup (b) Illustration of experimental paramters

Fig. 1. Illustration of modelling setup (model scale).

ground surface or buried at a depth d_f of 10 mm (model scale). All tests were performed at 68 g to simulate a prototype scenario in which a 6.1 m diameter tunnel with a cover depth $C = 8.0$ m was constructed beneath a 31.4 m wide building founded on 0.8 m wide footings with an embedment depth $d_f = 0$ or 0.7 m. The soil samples were prepared at 1 g by pouring the sand into the container in-line with the model tunnel and strip footings (for d_f =0.7 m) (see supplemental data for details). During the tests, tunnel volume loss $V_{l,t}$ was simulated by extracting water from the model tunnel in increments of 0.1% up to 3%; digital images of both the soil and the front face of the building model were taken at each increment.

EXPERIMENTAL RESULTS

Foundation displacements and ground deformations

The prototype scale settlements U_z and horizontal displacements U_x of the footings and underlying soil at $V_{l,t} = 2.0\%$ are plotted in Figures 2(a)-(b), along with greenfield soil displacements from Xu et al. (2020a); positive U_x and U_z are oriented towards the right and downwards, respectively. Additionally, Figure 2(c) presents the settlements of the central footing and greenfield soil, at the same location, against tunnel volume loss $V_{l,t}$. The greenfield settlements at $z = 0$ and 0.7 m do not differ drastically, with $i = 2.9$ m and $U_{z,max} = 31.4$ mm at $z = 0.7$ m, compared to $i = 3.4$ m, $U_{z,max} = 29.7$ mm at the surface, where i is the horizontal distance from the tunnel centerline to the inflection point of the settlement curve. In Figure 2, the apparent vertical penetration of the

footings into the underlying soil is due to the small gap between the front face of the model building and the acrylic wall of the strongbox (also observed in similar centrifuge tests by Farrell (2010); Ritter (2017)).

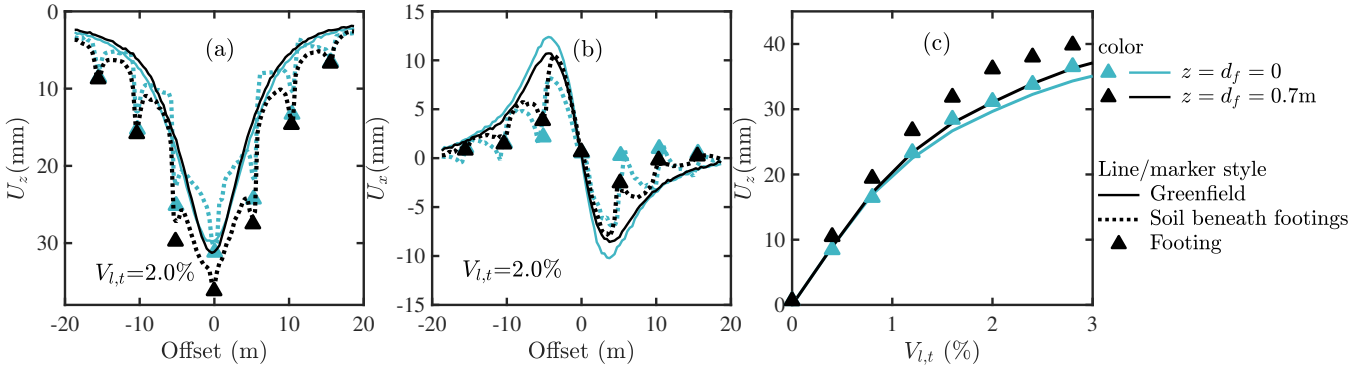

Fig. 2. Foundation and underlying soil displacements at $V_{l,t} = 2.0\%$ in (a) vertical and (b) horizontal directions; (c) central footings and corresponding greenfield settlements against $V_{l,t}$.

Results at $V_{l,t} = 2.0\%$ in Figure 2(a) show that the central footings (#3-5 from Figure 1) for $d_f = 0.7$ m settled more than for $d_f = 0$; the settlement of the external footings was similar for both d_f values. Consequently, the footing embedment d_f increased the building differential settlements. Figure 2(b) shows that footings restricted (compared to greenfield) the underlying soil horizontal displacements for all tests due to the stiffening action of the columns and the frictional interface between the soil and footings. The footing embedment d_f increased the level of differential horizontal displacements (therefore strains) between the footings. Figure 2(c) suggests that the settlements of the central footings are greater than the greenfield displacements in both tests, with a larger difference for the embedded foundation case. Furthermore, while for $d_f = 0$ the settlement increase with respect to the greenfield case occurs starting from $V_{l,t} = 1.0\%$, for $d_f = 0.7$ the difference can be observed from the very beginning of the test. Despite this, the structural stiffening action results in the reduction of building distortions compared to greenfield values, as discussed later.

Figure 3 presents contours of normalized ground horizontal (U_x/D_t) and vertical (U_z/D_t) displacements, along with engineering shear γ_s and volumetric ϵ_v strains of the soil at a tunnel volume loss of $V_{l,t} = 2.0\%$. In general, the greenfield results (from Xu et al. (2020b)) show: a chimney-like displacement pattern, as expected for the relatively low value of C/D_t (Marshall et al., 2012; Franza

et al., 2019); large shear strain zones at the tunnel shoulders; high levels of soil dilation directly above the tunnel crown; and intermediate levels of contraction within bands spanning from the tunnel springline to the surface. Comparing the case of footings resting on the surface (b) to greenfield (a) (as discussed in Xu et al. (2020b)): the footings restricted the horizontal displacements U_x of the soil with a distinct change in magnitude at the footing locations; settlements and shear strains above the tunnel crown are slightly decreased; localized zones of high shear strain are noted at the footing positions due to the action of the footings, resulting in dilation beneath the footings and contraction of the soil between footings.

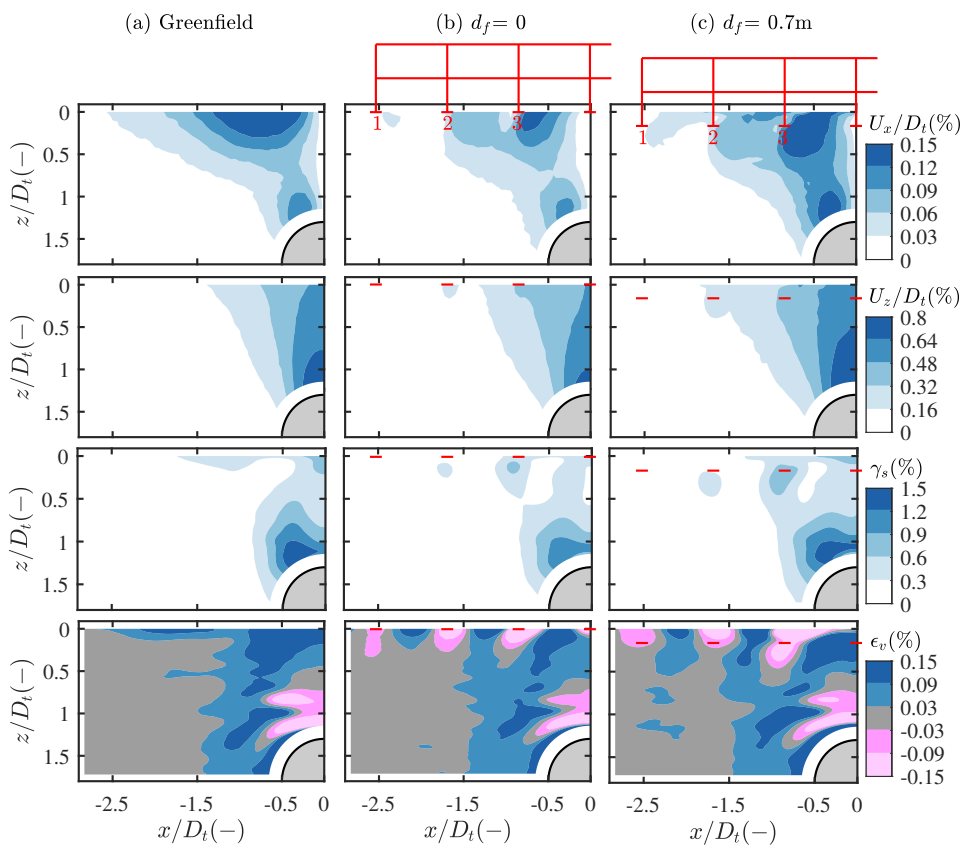

Fig. 3. Normalized soil displacements and strains at $V_{l,t}$ = 2.0% (ϵ_v<0 indicates dilation).

The role of footing embedment depth d_f is evaluated by comparing Figure 3(b)-(c). The embedded footings affected the displacements and strains of a much larger region of soil, with maximum soil displacements (both U_x and U_z) and engineering shear strains being greater for d_f = 0.7 m compared to d_f = 0. The pattern of U_x in the region between footings 1 and 2 is notable: for d_f = 0, U_x was negligible due to the actions of the footings, whereas for d_f = 0.7 m,

U_x is similar to the greenfield values in (a). The embedded footings are also seen to drag down the soil above the depth of 0.7 m, with equal magnitude soil settlements above the footings.

Structural deformations and level of damage

To consider the distribution of distortion and level of damage within panels, the deformed shape of the frames at $V_{l,t}$ = 2% is presented in Figure 4. Indicators are used for the range of maximum tensile strain ϵ_{max} and the category of damage within upper and lower panels to assess the distortion levels of panels. Values of ϵ_{max} were computed using the method of Elkayam and Klar (2019) using displacements at the four corners of a panel, while the category of damage was obtained from the thresholds of Boscardin and Cording (1989). A color scheme was adopted to denote low for category 0-1, medium for category 2 and high for category 3+.

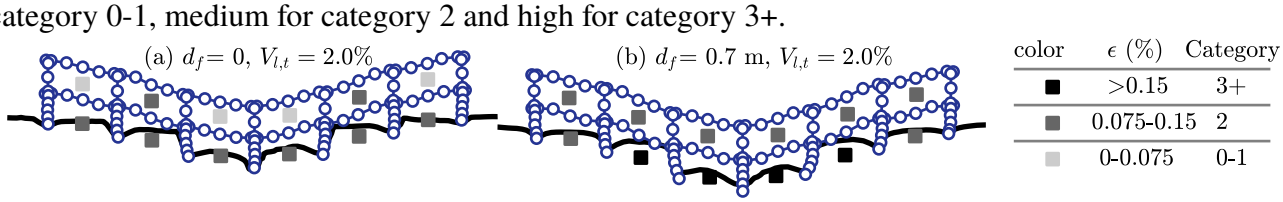

Fig. 4. Deformed shape and damage levels of the framed buildings at $V_{l,t}$ =2.0% (scale: 150).

For the frame with footings on the surface (d_f = 0), Figure 4(a) shows that, for the upper floor, only panel-2 and -5 underwent medium levels of damage, whereas all lower panels experienced medium damage levels due to the significant footing horizontal displacements (columns underwent bending deflections). For the embedded footings (d_f = 0.7 m) in (b), damage levels within both upper and lower level panels increased; for instance, all upper panels underwent medium levels of damage and the damage levels of the lower level panel-2 to -5 increased from medium to high. As illustrated in Figure 2, this is because the frame with embedded footings experienced greater differential settlements and horizontal displacements (larger bending deflections of columns) than the footings resting on the surface.

In practice, modification factor approaches are often used to predict tunneling-induced structure distortion from greenfield displacements. Xu et al. (2020a) and Goh and Mair (2014) presented modification factors of angular distortion M^{β} and horizontal strains $M^{\epsilon,h}$, respectively. For angular distortion, $M^{\beta} = \beta_{max}/\overline{GS}_{max}$ is obtained by normalizing the maximum angular distortion within the structures (β_{max}) by the maximum (among all bay locations) average slope of the greenfield

surface settlement trough spanning a bay width ($\overline{GS}_{max} = \Delta U_{z,gf,max}/b_{bay}$). The modification factor M^{β} was related to the relative soil-building shear stiffness $\kappa = (E_s B)/(GA_s^*)$, where E_s is the representative Young's modulus of the soil (estimated using the approach proposed by Farrell (2010);at $V_{l,t} = 1 - 2\%$, E_s is 90-61 MPa for $d_f = 0$ m, and 85-53 MPa for $d_f = 0.7$ m) and GA_s^* is the building shear stiffness per meter run (6.6E+05 N/m in model scale) obtained from loading tests using Timoshenko beam theory (the bending stiffness per meter run of the frame is 3.4E+04 Nm). Similarly, $M^{\epsilon,h} = \epsilon_{h,bldg}/\epsilon_{h,gf}$ is given by the ratio of the maximum horizontal strains ($\epsilon_{h,bldg,max}$) among all bays at the foundation level, to the maximum average horizontal strains ($\epsilon_{h,gf,max}$) inferred from the greenfield displacements at the footing locations. Following the work of Franza et al. (2017), the dimensionless relative footing-soil stiffness α_f^* is defined by $\alpha_f^* = 1/E_s \times 3K_b K_c/(h_{story}^2(2K_b + 3K_c))$ inferred from a one story, single bay portal (Goh and Mair, 2014), where $K_b = \left(EI/b_{bay}\right)_b$ = 1.4E+07 N and $K_c = \left(EI/h_{story}\right)_c$ = 2.7E+07 N are the average stiffness (per meter run) of the beam and footing column at prototype scale, respectively. The modification factors are plotted against relative stiffness in Figure 5 for $V_{l,t}$ = 0.5, 1.0 and 2.0%.

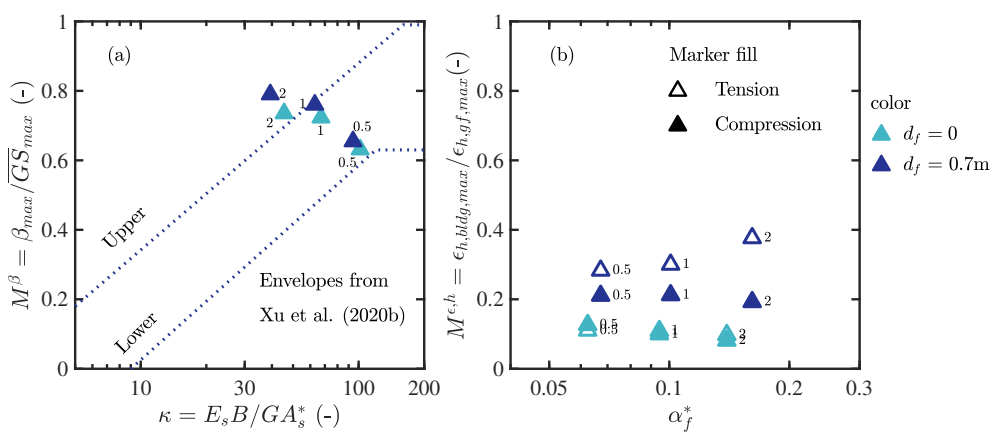

Fig. 5. Modification factors of (a) angular distortion and (b) horizontal strain against relative stiffness (numbers near markers indicate $V_{l,t}$).

Figure 5(a) shows that the impact of footing embedment on the normalized maximum angular distortion is minor, with the experimental results agreeing well with the empirical upper and lower envelopes (suggesting the maximum and minimum values of M^{β} for a given relative stiffness) proposed by Xu et al. (2020b), which were based on centrifuge test data for frames with footings on the ground surface, i.e. $d_f = 0$. The frame with embedded footings displays slightly larger

M^{β} values than the frame with footings on the surface, with the difference increasing with tunnel volume loss $V_{l,t}$. Figure 5(b) shows that the frame with embedded footings exhibits larger values of $M^{\epsilon,h}$ in both tensile and compressive deformation modes. Interestingly, results of the $d_f = 0$ test indicate that modification factors for the tensile and compressive strains are nearly identical, whereas for $d_f = 0.7$ m, larger values of $M^{\epsilon,h}$ are obtained for tension than for compression, likely due to the effect of active/passive earth pressures acting on the sides of the embedded footings. The reason for this different response between surface and embedded footings relates to a complex combination of mechanisms affecting the footing response, i.e. those related to the soil (e.g. shear resistance to sliding and active/passive earth pressures) and those related to the building (which would be consistent for the two cases considered). The experimental results do not enable a full understanding of how these complex mechanisms combine to produce the observed results; further study, perhaps with the use of numerical modeling, is required in this regard.

CONCLUSIONS

This technical note presented results from a centrifuge study on the effects of foundation embedment depth on tunneling-induced deformations of a framed building resting on separate footings. Results illustrated that the embedment slightly increased the ground deformations, the foundation differential settlements and the building (shear) angular distortions. On the other hand, the increase in tunneling-induced horizontal strains at the foundation was notable, particularly at high tunnel volume losses. Results were also used to evaluate frame modification factors, normalizing the building maximum angular distortion and maximum horizontal strains by the greenfield deformation levels.

The presented results indicate that, in practice, engineers should consider that the embedment of separate footings could increase tunneling-induced distress of buildings with respect to predictions obtained by assuming footings rest directly on the ground surface, particularly if the building is susceptible to the actions of horizontal ground deformations (as for separate footings). The presented results relate to a relatively shallow footing embedment (0.7 m); future work is planned to evaluate cases with deeper embedment.

DATA AVAILABILITY

Data are available from the authors on request.

REFERENCES

Boldini, D., Losacco, N., Bertolin, S., and Amorosi, A. (2018). "Finite Element modelling of tunnelling-induced displacements on framed structures." *Tunnelling and Underground Space Technology*, 80(Oct), 222–231.

Boscardin, M. D. and Cording, E. J. (1989). "Building response to excavation-induced settlement." *Journal of Geotechnical Engineering*, 115(1), 1–21.

Elkayam, I. and Klar, A. (2019). "Nonlinear elasto-plastic formulation for tunneling effects on superstructures." *Canadian Geotechnical Journal*, 56(7), 956–969.

Ellis, E., Cox, C., Yu, H. S., Ainsworth, A., and Baker, N. (2006). "A new geotechnical centrifuge at the University of Nottingham, UK." *6th International Conference of Physical Modelling in Geotechnics: ICPMG'06*, Ng, Zhang, and Wang, eds., Hong Kong, Taylor & Francis Group, London, 129–133.

Farrell, R. (2010). "Tunnelling in sands and the response of buildings." *Ph.D. Thesis, Cambridge University*.

Franza, A., Marshall, A. M., Haji, T., Abdelatif, A. O., Carbonari, S., and Morici, M. (2017). "A simplified elastic analysis of tunnel-piled structure interaction." *Tunnelling and Underground Space Technology*, 61, 104–121.

Franza, A., Marshall, A. M., and Zhou, B. (2019). "Greenfield tunnelling in sands: the effects of soil density and relative depth." *Géotechnique*, 69(4), 297–307.

Fu, J., Yu, Z., Wang, S., and Yang, J. (2018). "Numerical analysis of framed building response to tunnelling induced ground movements." *Engineering Structures*, 158(Mar), 43–66.

Goh, K. H. and Mair, R. J. (2014). "Response of framed buildings to excavation-induced movements." *Soils and Foundations*, 54(3), 250–268.

Lanzano, G., Visone, C., Bilotta, E., and Santucci de Magistris, F. (2016). "Experimental Assessment of the Stress–Strain Behaviour of Leighton Buzzard Sand for the Calibration of a Constitutive Model." *Geotechnical and Geological Engineering*, 34(4), 991–1012.

Losacco, N., Burghignoli, A., and Callisto, L. (2014). "Uncoupled evaluation of the structural damage induced by tunnelling." *Géotechnique*, 64(8), 646–656.

Marshall, A. M., Farrell, R., Klar, A., and Mair, R. (2012). "Tunnels in sands: the effect of size, depth and volume loss on greenfield displacements." *Géotechnique*, 62(5), 385–399.

Ritter, S. (2017). "Experiments in tunnel-soil-structure interaction." *Ph.D. thesis, University of Cambridge*.

White, D., Take, W., and Bolton, M. (2003). "Soil deformation measurement using particle image velocimetry (PIV) and photogrammetry." *Géotechnique*, 53(7), 619–631.

Xu, J., Franza, A., and Marshall, A. M. (2020a). "Response of framed building on raft foundations to tunneling." *Journal of Geotechnical and Geoenviromental Engineering*, 146(11), 04020120.

Xu, J., Franza, A., Marshall, A. M., Losacco, N., and Boldini, D. (2020b). "Tunnel-framed building interaction: comparison between raft and separate footing foundations." *Géotechnique (in press)*.

Yiu, W. N., Burd, H. J., and Martin, C. M. (2017). "Finite-element modelling for the assessment of tunnel-induced damage to a masonry building." *Géotechnique*, 67(9), 780–794.

Zhao, Y. (2008). "In situ soil testing for foundation performance prediction." *Ph.D. Thesis, Cambridge University*.

SUPPLEMENTAL DATA

Preparation of the soil sample

The soil samples were prepared at 1 g by pouring the sand into the container in-line with the model tunnel; for this, the strongbox was placed with the front acrylic wall resting on the floor. When testing the foundation resting directly on the surface, the building model was placed at 1 g on the surface after sand pouring. A more elaborate preparation methodology was needed to achieve uniform ground conditions in the embedded footing test. As shown in Figure S1(a), the building model was placed inside the strongbox prior to sample preparation, and sand was poured in-line with the longitudinal direction of the footings and tunnel. To set the ground level above the footings, two temporary aluminum plates were placed on each side of the building model, whereas acrylic plates were placed inside each panel of the first story. A temporary wooden plate was also fixed to the strongbox to provide lateral support to the temporary side plates and the building model. For each acrylic plate, the lateral support was applied by two threaded rods drilled through the building floors, which were in-turn supported by the temporary wooden plate. Thin foam tape was attached in the gap between the temporary plates and strongbox/footings to prevent sand leakage. After sand pouring, the back wall was attached and the strongbox was rotated to the upright position, with temporary supports subsequently removed. To avoid the interaction between acrylic plates and the soil surface within building panels during tests, the plates were pulled up using the threaded rods and hung from the top aluminum plates (see Figure S1(b)). Once raised, there was a 2 mm gap between the acrylic plates and the footing walls, ensuring the acrylic plates did not affect the horizontal displacements of the footings during tests (they contributed slightly to the building weight).

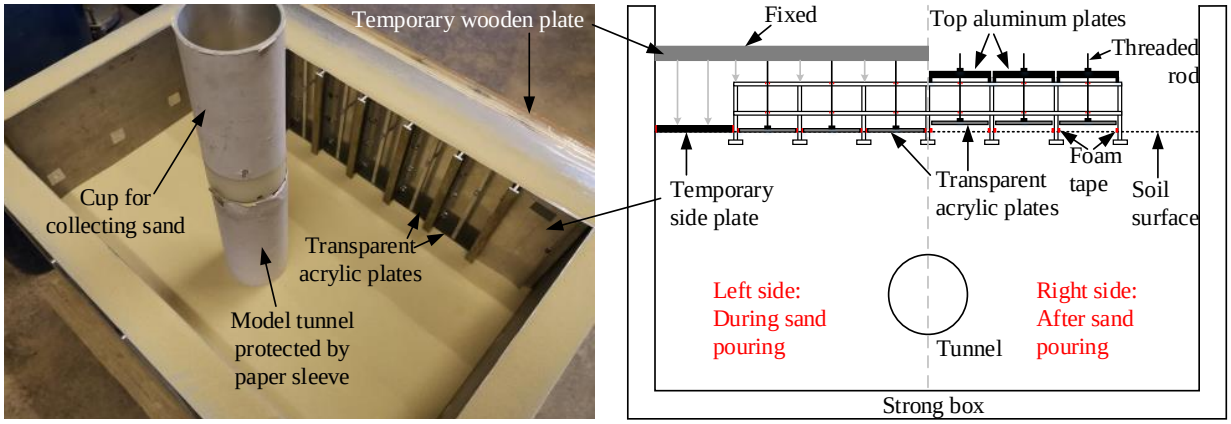

(a) Sand pouring (b) Illustration of sand pouring process

Fig. S1. Illustration of sand pouring process.